CRYSTAL GROWTH & DESIGN

Article

pubs.acs.org/crystal

Diverse Topologies in Chiral Divalent Metal Camphorate Coordination Polymers Containing 4,4′-Dipyridylamine

Karyn M. Blake, Chaun M. Gandolfo, Jacob W. Uebler, and Robert L. LaDuca*

Lyman Briggs College and Department of Chemistry, Michigan State University, East Lansing, Michigan 48825, United States

Supporting Information

ABSTRACT: Hydrothermal synthesis has afforded six chiral divalent metal coordination polymers containing D-camphorate (D-cmph) and 4,4′-dipyridylamine (dpa) ligands, whose topologies depend largely on metal coordination geometry preference. Both cadmium derivatives $\{[Cd(dpa)(D\text{-}cmphH)_2(H_2O)]\cdot 0.875H_2O\}_n$ (**1**) and $\{[Cd(D\text{-}cmph)(dpa)(Hdpa)]ClO_4\}_n$ (**1a**) exhibit one-dimensional (1-D) chains with protonated pendant ligands; **1** possesses sinusoidal chains with a "wavelength" of over 67 Å. $[Zn_2(D\text{-}cmph)_2(dpa)(H_2O)]_n$ (**2**) exhibits a two-dimensional (2-D) 3,4-connected binodal net with $(5^3)_2(5^48^2)$ topology. $\{[Ni(D\text{-}cmph)(dpa)]\cdot 3H_2O\}_n$ (**3**) and $\{[M_2(D\text{-}cmph)_2(dpa)]\cdot H_2O\}_n$ (M = Co, **4**; M = Cu, **5**) manifest three-dimensional (3-D) networks. The nickel derivative has an uncommon 2-fold interpenetrated 4-connected 4^28^4 **lvt** topology, while the isostructural cobalt and copper complexes possess 6-connected **pcu** topologies based on $\{M_2(OCO)_4\}$ paddlewheel dimers. Complexes **1**/**1a** and **2** undergo visible light emission upon ultraviolet excitation. Variable temperature magnetic susceptibility experiments indicate weak ($J = -3.6(2)$ cm^{-1}) and strong ($J = -202(5)$ cm^{-1}) antiferromagnetic coupling for **4** and **5**, respectively.

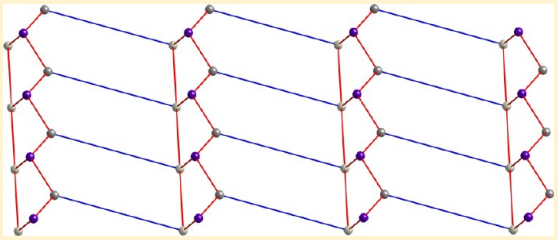

INTRODUCTION

The synthesis and characterization of divalent metal coordination polymers remain under focused investigation, with efforts geared toward the design of crystalline materials tailored to industrially relevant hydrogen storage,[1] molecular separation,[2] ion exchange,[3] catalysis,[4] and nonlinear optical applications.[5] Dicarboxylate ligands are certainly the most commonly employed linkers in the construction of these materials. The geometric orientation of carboxylate donors, specific divalent metal coordination environments, and various carboxylate binding modes provide a plethora of diverse structural topologies.[6] Additionally, carboxylate bridges can instill spin communication and temperature- and field-dependent magnetic properties in these extended solids,[7] which depend heavily on the overlap and interaction of the magnetic orbitals on neighboring paramagnetic metal ions.

Chiral coordination polymers have seen recent interest as substrates for enantioselective catalysis or separations.[8] For instance, Lin and co-workers used a chiral dipyridyl-type ligand to prepare a 2-fold interpenetrated three-dimensional (3-D) cadmium coordination polymer. After postsynthetic treatment with titanium isopropoxide, it catalyzed the formation of chiral secondary alcohols from aromatic aldehydes and diethylzinc with both high conversion and enantiomeric excess.[8a] Rosseinsky and others have prepared the 3-D chiral coordination polymer $[Ni_2(L\text{-aspartate})_2(4\text{-bpy})]_n$ (4-bpy = 4,4′-bipyridine), which can serve as the solid phase for the gas chromatographic separation of aliphatic diol enantiomers.[8b]

Chiral coordination polymers can be synthesized by utilizing enantiopure dicarboxylate ligands such as D-camphorate (D-cam), either in the presence[9] or absence[10] of a neutral dipyridyl coligand.

Scheme 1. Ligands Used in This Study

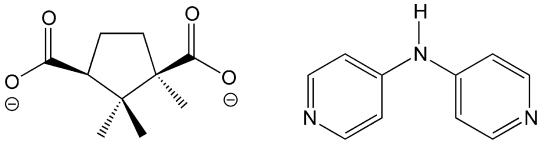

Bu and colleagues prepared three different 3-D cadmium D-camphorate coordination polymers, simply by varying the synthesis temperature and eschewing any coligands.[10] Metal-dependent topological control has been seen in dual-ligand D-cam coordination polymers; for instance, $[Ni(D\text{-}cam)(dpp)]_n$ (dpp = 1,3-di-4-pyridylpropane) exhibits a very rare chiral two-dimensional (2-D) bilayer structure with 4^26^38 topology, while $\{[Co(D\text{-}cam)(dpp)]\cdot H_2O\}_n$ has a chiral 3-fold interpenetrated 6^6 topology diamondoid net.[9a] $\{[Cd(D\text{-}cam)(dpp)]\cdot 2H_2O\}_n$ has a similar topology to its cobalt analogue, but dehydration and further heating result in a single crystal-to-single crystal structural reorganization due to twists and compressions of the helical subunits in the solid state.[9b]

An alternative method of generating chiral coordination polymers has been through the spontaneous resolution of locked conformations of otherwise achiral ligands.[11] The kinked dipyridyl ligand 4,4′-dipyridylamine (dpa) has proven an effective choice for this approach, as twists between the two

Received: July 31, 2012
Revised: August 25, 2012
Published: August 28, 2012

Table 1. Crystal and Structure Refinement Data for 1−5

data	1	1a	2	3	4	5
empirical formula	$C_{180}H_{253}Cd_6N_{18}O_{57.5}$	$C_{30}H_{33}CdClN_6O_8$	$C_{60}H_{78}N_6O_{18}Zn_4$	$C_{80}H_{116}N_{12}Ni_4O_{28}$	$C_{30}H_{39}Co_2N_3O_9$	$C_{30}H_{39}Cu_2N_3O_9$
formula weight	4263.44	753.47	1432.76	1924.69	703.50	712.72
crystal system	monoclinic	orthorhombic	monoclinic	orthorhombic	monoclinic	monoclinic
space group	$P2_1$	$P2_12_12$	$P2_1$	$P2_12_12$	$C2$	$C2$
Flack parameter	−0.01(2)	0.05(5)	0.010(12)	0.076(17)	0.25(4)	0.37(3)
a (Å)	12.2428(8)	19.0413(19)	9.2562(6)	19.261(2)	19.028(3)	18.868(6)
b (Å)	67.775(5)	23.213(2)	14.3930(10)	34.341(4)	12.8531(17)	12.860(4)
c (Å)	12.2969(8)	7.1223(7)	24.2543(17)	13.6935(15)	13.5044(18)	13.360(4)
β (°)	107.103(1)	90	90.878(1)	90	105.871(2)	106.562(6)
V (Å^3)	9752.2(11)	3148.1(5)	3230.9(4)	9057.7(17)	3176.9(7)	3107.3(18)
Z	2	4	2	4	4	4
D_{calc} (g cm^{-3})	1.446	1.590	1.473	1.375	1.471	1.524
μ (mm^{-1})	0.728	0.839	1.540	0.897	1.101	1.426
min/max trans.	0.8035/0.9222	0.8337/0.9238	0.7722/0.8637	0.7969/0.9531	0.8165/0.9017	0.6621/0.8800
hkl ranges	$-14 \le h \le 14$	$-22 \le h \le 22$	$-13 \le h \le 13$	$-23 \le h \le 22$	$-22 \le h \le 22$	$-22 \le h \le 22$
	$-80 \le k \le 81$	$-27 \le k \le 26$	$-14 \le k \le 14$	$-41 \le k \le 41$	$-15 \le k \le 15$	$-15 \le k \le 15$
	$-14 \le l \le 14$	$-8 \le l \le 8$	$-26 \le l \le 25$	$-16 \le l \le 16$	$-16 \le l \le 16$	$-16 \le l \le 16$
total reflections	80542	19362	47555	106491	22961	22122
unique reflections	35532	5685	11800	16642	5794	5724
R(int)	0.0905	0.0529	0.0826	0.1086	0.0727	0.0726
parameters/restraints	2188/15	428/3	823/9	1019/0	381/9	399/4
R_1 (all data)[a]	0.1077	0.0584	0.0608	0.0949	0.0943	0.1194
R_1 ($I > 2\sigma(I)$)	0.0712	0.0493	0.0514	0.0788	0.0679	0.0803
wR_2 (all data)[b]	0.1687	0.1375	0.1310	0.2235	0.1930	0.2501
wR_2 ($I > 2\sigma(I)$)	0.1495	0.1317	0.1253	0.2109	0.1731	0.2245
max/min residual (e$^-$/Å^3)	1.559/−0.942	0.925/−1.085	0.876/−0.761	1.611/−0.912	0.703/−0.401	0.570/−1.200
GOF	1.039	1.056	1.080	0.993	1.041	1.068

[a] $R_1 = \Sigma||F_o| - |F_c||/\Sigma|F_o|$. [b] $wR_2 = \{\Sigma[w(F_o^2 - F_c^2)^2]/\Sigma[wF_o^2]^2\}^{1/2}$.

pyridyl rigands of dpa have imparted helical substructures in the chiral materials $\{[Cd(pht)(dpa)]\cdot 4H_2O\}_n$ (pht = phthalate) and $\{[Cu_2(pth)_2(dpa)]\cdot H_2O\}_n$.[11a,b] These two phases adopt extremely rare topologies, showing a 4-connected 3-D self-penetrated 7^48^2 **yyz** net and a 4-connected one-dimensional (1-D) linked septuple helix nanobarrel motif, respectively. In this study we aimed to explore and compare the structures of divalent metal coordination polymer phases incorporating both the D-cam and dpa ligands (Scheme 1). Herein we report the synthesis, structural characterization, and some preliminary physical property studies for six new chiral coordination polymers: $\{[Cd(dpa)(D\text{-cmphH})_2(H_2O)]\cdot 0.875H_2O\}_n$ (**1**), $\{[Cd(D\text{-cmph})(dpa)(Hdpa)]ClO_4\}_n$ (**1a**), $[Zn_2(D\text{-cmph})_2(dpa)(H_2O)]_n$ (**2**), $\{[Ni(D\text{-cmph})(dpa)]\cdot 3H_2O\}_n$ (**3**), and $\{[M_2(D\text{-cmph})_2(dpa)]\cdot H_2O\}_n$ (M = Co, **4**; M = Cu, **5**).

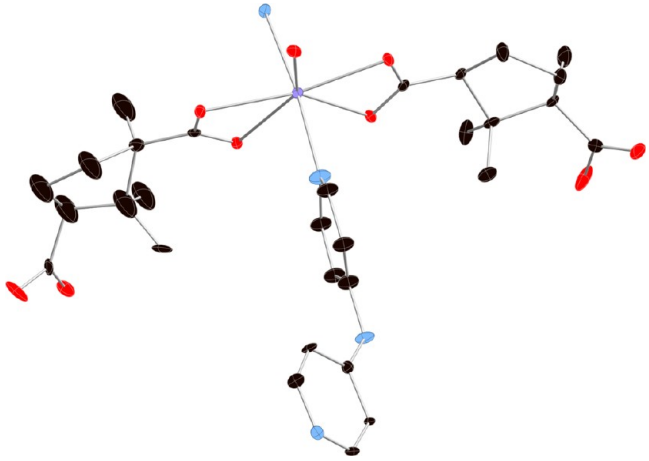

Figure 1. A representative coordination environment in **1**.

EXPERIMENTAL SECTION

General Considerations. Metal salts were purchased from Aldrich. D-Camphoric acid was purchased from TCI America. 4,4′-Dipyridylamine (dpa) was prepared using a published procedure.[12] Water was deionized above 3 MΩ-cm in-house. IR spectra were recorded on powdered samples using a Perkin-Elmer Spectrum One instrument. Variable temperature magnetic susceptibility data for **4** and **5** (2−300 K) were collected on a Quantum Design MPMS SQUID magnetometer at an applied field of 0.1 T. After each temperature change the sample was kept at the new temperature for 5 min before magnetization measurement to ensure thermal equilibrium. The susceptibility data was corrected for diamagnetism using Pascal's constants,[13] and for the diamagnetism of the sample holder. The luminescence spectra of **1**/**1a** and **2** were obtained with a Hitachi F-4500 Fluorescence spectrometer on solid crystalline samples anchored to quartz microscope slides with Rexon Corporation RX-22P ultraviolet-transparent epoxy adhesive. Thermogravimetric analysis was performed on a TA Instruments high-resolution Q500 thermal analyzer under flowing N_2.

Preparation of $\{[Cd(dpa)(D\text{-cmphH})_2(H_2O)]\cdot 0.875H_2O\}_n$ (1) and $\{[Cd(D\text{-cmph})(dpa)(Hdpa)]ClO_4\}_n$ (1a). $Cd(ClO_4)_2\cdot 6H_2O$ (59 mg, 0.14 mmol), dpa (60 mg, 0.35 mmol), and D-camphoric acid (33 mg, 0.17 mmol) were placed into 10 mL of distilled H_2O in a 23 mL Teflon-lined Parr acid digestion bomb. The bomb was sealed and heated at 120 °C for 48 h, whereupon it was cooled slowly to 25 °C. A mixture of slightly yellow and colorless blocks of **1** and **1a** were isolated after washing with distilled water, acetone, and drying in air. The blocks of **1** and **1a** could be distinguished by their visual appearance, but manual separation proved impractical. Attempts to prepare **1** and **1a** in phase pure fashion via adjustment of precursor stoichiometry and

dx.doi.org/10.1021/cg301091f | Cryst. Growth Des. 2012, 12, 5125−5137

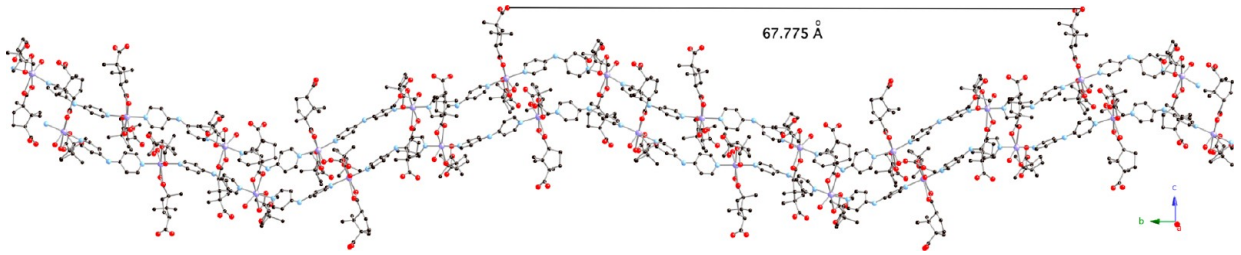

Figure 2. A pair of crystallographically distinct $\{[Cd(dpa)(D\text{-}cmphH)_2(H_2O)]\}_n$ 1-D chains in **1**.

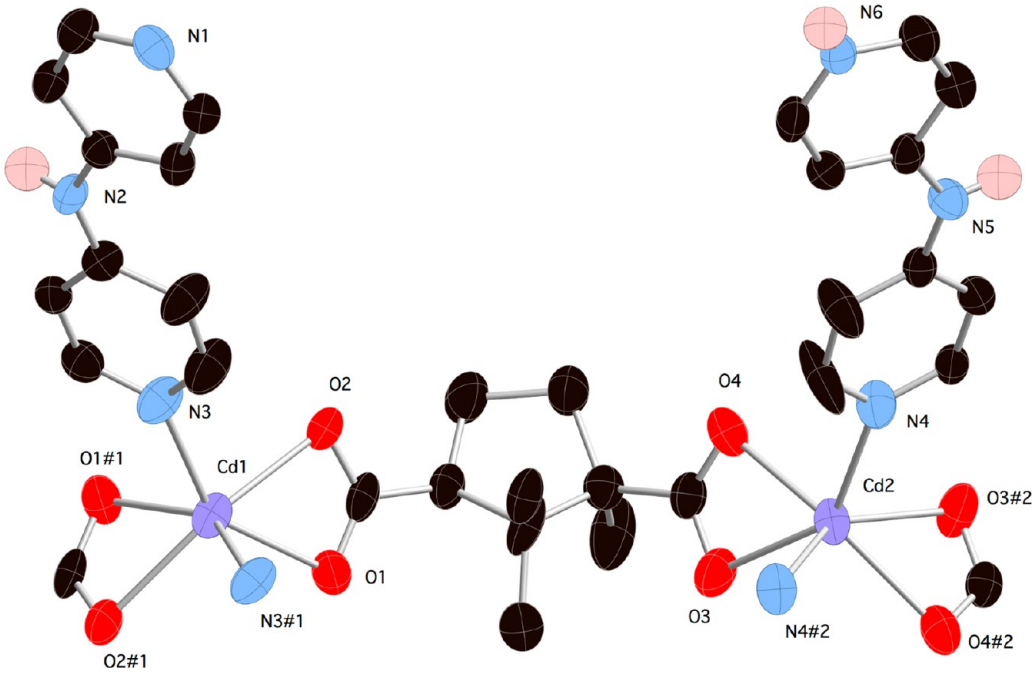

Figure 3. Coordination environments of **1a**.

synthesis temperature proved fruitless. IR for the solid multiphase mixture (cm^{-1}): 3423 (w), 2968 (w), 1684 (w), 1591 (m), 1522 (s), 1441 (w), 1405 (m), 1344 (m), 1300 (w), 1212 (s), 1161 (w), 1116 (w), 1080 (s) 1011 (m), 928 (w), 904 (w), 820 (m), 731 (w).

Preparation of $[Zn_2(D\text{-}cmph)_2(dpa)(H_2O)]_n$ (2). $ZnSO_4{\cdot}7H_2O$ (58 mg, 0.20 mmol), dpa (60 mg, 0.35 mmol), and D-camphoric acid (36 mg, 0.18 mmol) were placed into 10 mL of distilled H_2O in a 23 mL Teflon-lined Parr acid digestion bomb. The bomb was sealed and heated at 120 °C for 48 h, whereupon it was cooled slowly to 25 °C. Colorless blocks of **2** (36 mg, 0.050 mmol, 56% yield) were isolated after washing with distilled water, acetone and drying in air. Anal. Calc. for $C_{60}H_{78}N_6O_{18}Zn_4$ **2**: C, 50.29; H, 5.49; N, 5.87% Found: C, 50.33; H, 4.82; N, 5.87%. IR (cm^{-1}): 3300 (w, br), 2941 (sb), 1405 (s), 1552 (s), 1525 (s), 1448 (m), 1384 (s), 1360 (s), 1211 (s), 1059 (w), 1026 (s), 910 (m), 821 (s).

Preparation of $\{[Ni(D\text{-}cmph)(dpa)]{\cdot}3H_2O\}_n$ (3). $NiCl_2{\cdot}6H_2O$ (56 mg, 0.19 mmol), dpa (62 mg, 0.36 mmol), and D-camphoric acid (32 mg, 0.16 mmol) were placed into 10 mL of distilled H_2O in a 23 mL Teflon-lined Parr acid digestion bomb. The bomb was sealed and heated at 120 °C for 48 h, whereupon it was cooled slowly to 25 °C. Green blocks of **3** (48 mg, 0.10 mmol, 62% yield based on Ni) were isolated after washing with distilled water, acetone, and drying in air. Anal. Calc. for $C_{80}H_{116}N_{12}Ni_4O_{28}$ **3**: C, 49.82; H, 6.06; N, 8.72% Found: C, 49.80; H, 5.70; N, 8.63%. IR (cm^{-1}): 3400 (w, br), 2947 (m), 1574 (s), 1520 (s), 1397 (s), 1354 (s), 1212 (s), 1127 (m), 1042 (m), 1027 (m), 1007 (m), 904 (m), 845 (m), 809 (s).

Preparation of $\{[Co_2(D\text{-}cmph)_2(dpa)]{\cdot}H_2O\}_n$ (4). $Co(NO_3)_2{\cdot}6H_2O$ (55 mg, 0.18 mmol), dpa (60 mg, 0.35 mmol), and D-camphoric acid (35 mg, 0.17 mmol) were placed into 10 mL of distilled H_2O in a 23 mL Teflon-lined Parr acid digestion bomb. The bomb was sealed and heated at 120 °C for 48 h, whereupon it was cooled slowly to 25 °C. Magenta blocks of **4** (28 mg, 0.040 mmol, 47% yield based on Co) were isolated after washing with distilled water, acetone and drying in air. Anal. Calc. for $C_{30}H_{39}Co_2N_3O_9$ **4**: C, 51.22; H, 5.59; N, 5.97% Found: C, 51.28; H, 5.08; N, 5.93%. IR (cm^{-1}): 3433 (w), 2964 (w), 1587 (s), 1522 (s), 1489 (w), 1403 (s), 1355 (s), 1290 (w), 1214 (s), 1123 (w), 1060 (w), 1022 (s), 867 (s), 807 (s), 690 (w).

Preparation of $\{[Cu_2(D\text{-}cmph)_2(dpa)]{\cdot}H_2O\}_n$ (5). $CuSO_4{\cdot}5H_2O$ (41 mg, 0.16 mmol), dpa (60 mg, 0.35 mmol), and D-camphoric acid (34 mg, 0.17 mmol) were placed into 10 mL of distilled H_2O in a 23 mL Teflon-lined Parr acid digestion bomb. The bomb was sealed and heated at 120 °C for 48 h, whereupon it was cooled slowly to 25 °C. Green blocks of **5** (36 mg, 0.051 mmol, 64% yield based on Cu) were isolated after washing with distilled water, acetone, and drying in air. Anal. Calc. for $C_{30}H_{39}Cu_2N_3O_9$ **5**: C, 50.56; H, 5.52; N, 5.90% Found: C, 50.47; H, 5.03; N, 5.75%. IR (cm^{-1}): 3463 (w), 2967 (w), 1574 (s), 1515 (s), 1491 (w), 1398 (s), 1355 (s), 1295 (w), 1214 (s), 1173 (w), 1127 (w), 1062 (w), 1027 (m), 1008 (m), 953 (w), 906 (w), 846 (w), 810 (s), 787 (m), 663 (w).

X-ray Crystallography. Single crystal X-ray diffraction was performed on crystals of **1**–**5** using a Bruker-AXS ApexII CCD instrument at 173 K. Reflection data were acquired using graphite–monochromated Mo–Kα radiation (λ = 0.71073 Å). The data were integrated via SAINT.[14] Lorentz and polarization effect and empirical absorption corrections were applied with SADABS.[15] The structures were solved using direct methods and refined on F^2 using SHELXTL.[16] All non-hydrogen atoms were refined anisotropically.

dx.doi.org/10.1021/cg301091f | Cryst. Growth Des. 2012, 12, 5125–5137

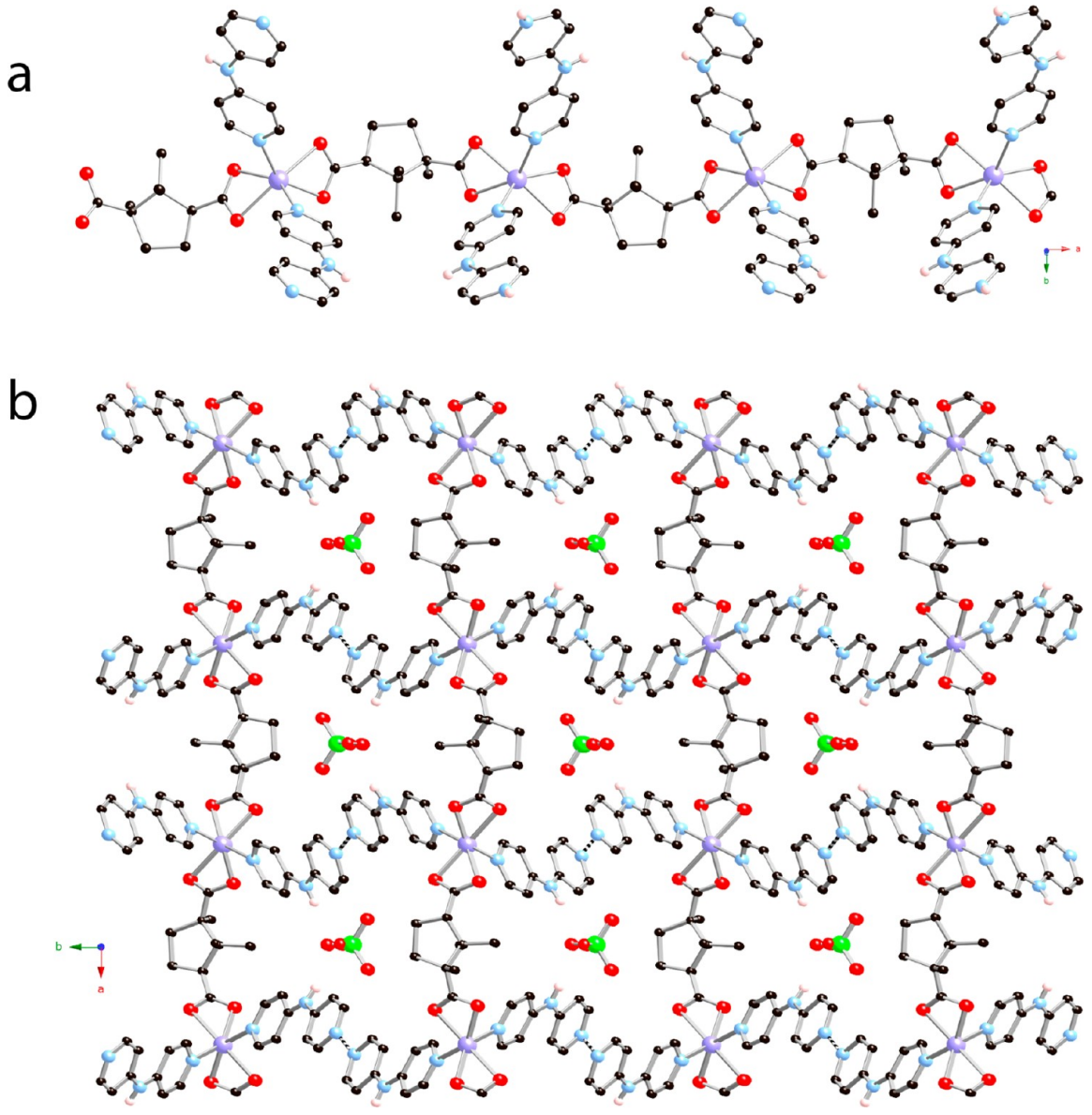

Figure 4. (a) 1-D chain motif in **1a**. (b) Stacked supramolecular layers in **1a** with embedded perchlorate counterions. Hydrogen bonding is shown as dashed lines.

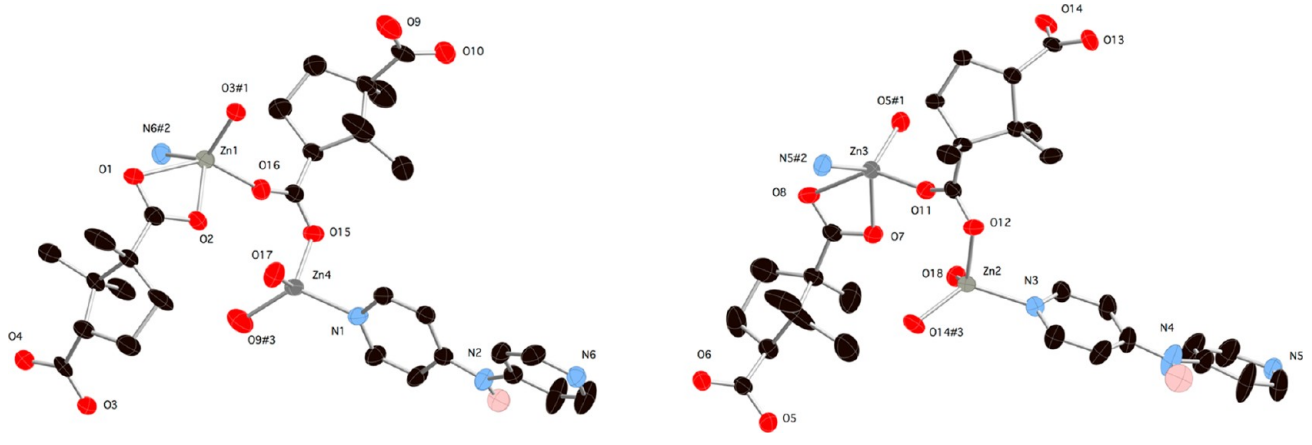

Figure 5. Coordination environments of **2**.

Hydrogen atoms bound to carbon atoms were placed in calculated positions and refined isotropically with a riding model. The hydrogen atoms of the dpa amine group and most of the ligated water molecules were found via Fourier difference maps, and then restrained at fixed

dx.doi.org/10.1021/cg301091f | *Cryst. Growth Des.* 2012, 12, 5125−5137

Scheme 2. Binding Modes of the D-Camphorate Ligands in 1−5

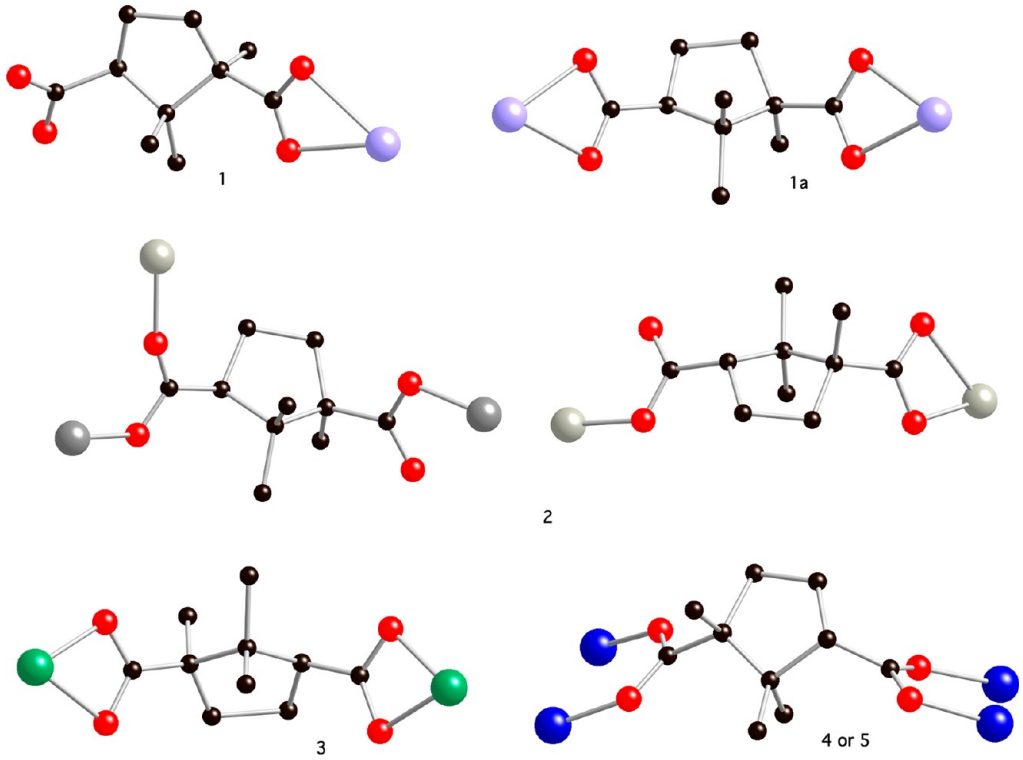

positions and refined isotropically. Some distended thermal ellipsoids in **1** likely indicate some unresolvable crystallographic disorder. The electron density of the highly disordered water molecules in **3** was accounted for using the SQUEEZE program.[17] Some racemic twinning was evident in the crystals of **4** and **5**. Higher than expected R_1 and wR_2 statistics for **5** are attributed to some racemic twinning and small crystal size. Relevant crystallographic data for **1**−**5** are listed in Table 1, with racemic purity within the crystal evaluated by the Flack parameter.[18] Topological analyses were carried out using TOPOS software.[19]

RESULTS AND DISCUSSION

Synthesis and Spectral Characterization. Compounds **1**−**5** were prepared as crystalline products by hydrothermal reaction of the appropriate metal salt, D-camphoric acid, and 4,4′-dipyridylamine. The infrared spectra of **1**−**5** were consistent with their structural characteristics as determined by single−crystal X−ray diffraction. Weak and medium intensity bands in the range of ∼1600 cm^{-1} to ∼1200 cm^{-1} can be ascribed to stretching modes of the pyridyl rings of nitrogen−base ligands. Puckering modes of the pyridyl rings are evident in the region between 820 cm^{-1} and 600 cm^{-1}. Asymmetric and symmetric C−O stretching modes of the carboxylate groups of fully deprotonated D-cmph ligands correspond to the strong, broadened features at 1522 cm^{-1} and 1405 cm^{-1} (for **1**/**1a**), 1556 cm^{-1} and 1360 cm^{-1} (for **2**), 1574 cm^{-1} and 1397 cm^{-1} (for **3**), 1578 cm^{-1} and 1402 cm^{-1} (for **4**), and 1574 cm^{-1} and 1397 cm^{-1} (for **5**). Broad yet weak bands in the region of ∼3400 cm^{-1} to ∼3200 cm^{-1} represent N−H stretching modes within the dpa ligands and O−H bonds within ligated and/or unbound water molecules in **2**−**5**. The broadness of these higher energy spectral features is caused by the hydrogen bonding present in all cases. The perchlorate ion in **1a** was denoted by the very strong band at 1080 cm^{-1}.

Structural Description of $\{[Cd(dpa)(D\text{-}cmphH)_2(H_2O)]\cdot 0.875H_2O\}_n$ (1). The extremely large asymmetric unit of compound **1** contains 6 crystallographically distinct divalent cadmium atoms, 6 dpa ligands, 12 pendant and protonated D-cmphH ligands, 6 aqua ligands, and 4 water molecules of crystallization, one of which refined at half-occupancy. A distorted $\{CdO_5N_2\}$ pentagonal bipyramidal coordination environment (Figure 1) is present at all cadmium atoms, with *trans* dpa pyridyl nitrogen donor atoms in the axial positions. The equatorial plane consists of the aqua ligand and chelating carboxylate groups from two different pendant, protonated D-cmphH ligands. Crystallographic distinction is fostered by subtle conformational variances within the dpa and D-cmphH ligands, and binding modes of the D-cmphH ligands. Bond lengths and angles within a representative coordination sphere in **1** are listed in Table S1. Other coordination spheres within **1** are largely identical.

Cadmium atoms are linked into undulating $\{[Cd(dpa)(D\text{-}cmphH)_2(H_2O)]_n$ 1-D chains, coincident with the 2_1 screw axes along the *b* crystal direction (Figure 2). Sets of three crystallographically distinct cadmium with attendant ligands produce two crystallographically distinct $\{[Cd(dpa)(D\text{-}cmphH)_2(H_2O)]_n$ 1-D chains. In one chain (chain-A with Cd2, Cd5, Cd6) the Cd···Cd through-ligand distances measure 11.861, 11.928, and 11.970 Å, while in the other (chain-B with Cd1, Cd3, Cd4) these distances are 12.219, 11.880, and 11.937 Å. Variances in these distances are fostered by differences in the inter-ring torsion angles within the dpa ligands. Additionally, the pendant D-cmph ligands bind in different orientations depending on the specific cadmium atom to which they are ligated, resulting in crystallographic distinction between chain-A and chain-B. In chain-A, both chelating groups bound to Cd2 belong to methylated carboxylate termini of the D-cmphH ligands, while all chelating groups bound to Cd6 and Cd5

dx.doi.org/10.1021/cg301091f | *Cryst. Growth Des.* 2012, 12, 5125−5137

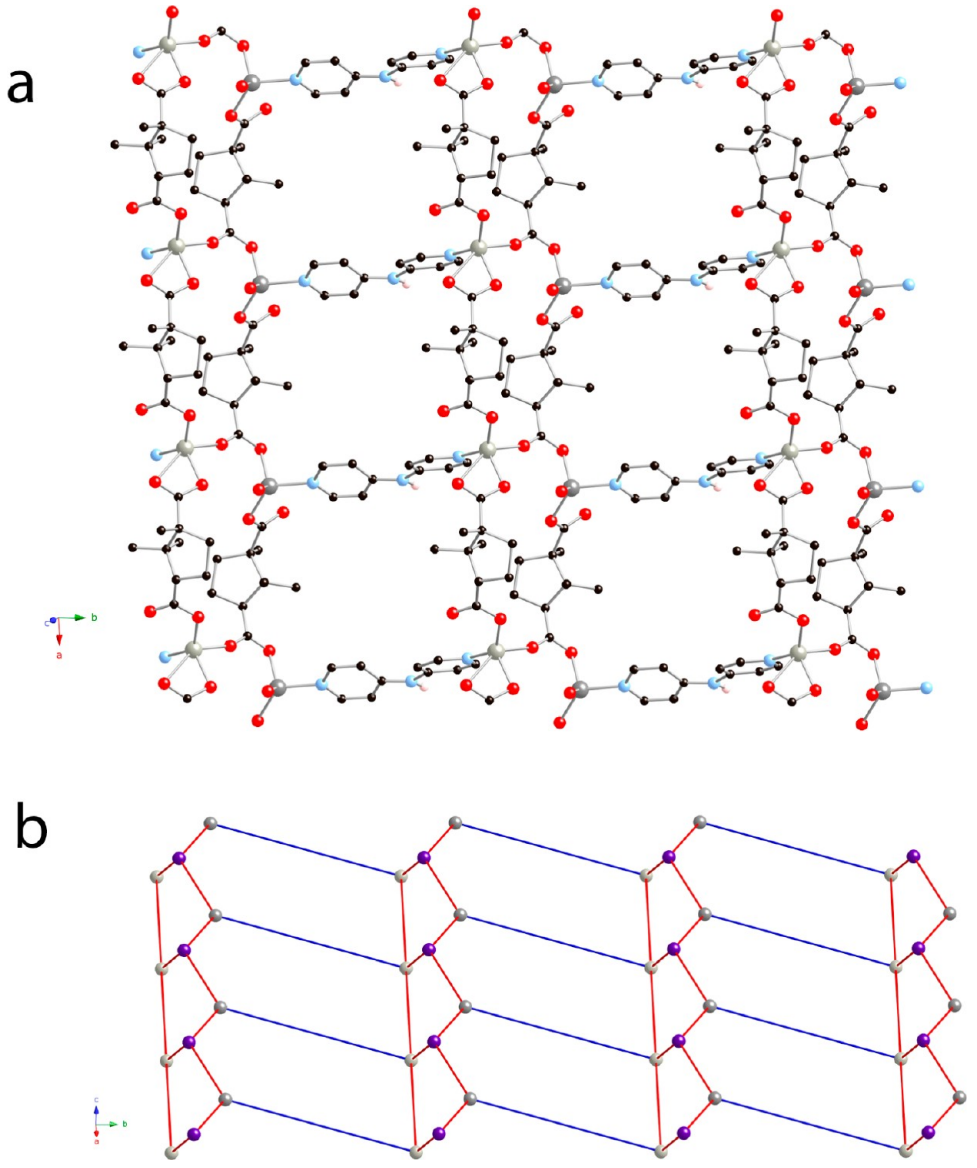

Figure 6. (a) 2-D layer motif in **2**. (b) 3,4-connected binodal net with $(5^3)_2(5^48^2)$ topology in **2**. The gray and violet spheres represent zinc atoms and exotridentate D-cmph ligands, respectively.

belong to hydrogenated carboxylate termini of the D-cmphH ligands. In chain-B, both chelating groups bound to Cd3 belong to methylated carboxylate termini of the D-cmphH ligands, while the chelating groups bound to Cd1 and Cd4 are split; one chelating group on each belongs to a methylated D-cmphH carboxylate, while the other belongs to a hydrogenated D-cmphH carboxylate.

The "wavelength" of the sinusoidal 1-D chains is a rather long 67.775 Å, marking the *b* lattice parameter. Neighboring chains are anchored into a 2-D supramolecular layer by hydrogen bonding donation from dpa central amine groups to ligated carboxylate oxygen atoms of the D-cmphH ligands (Figure S1, Supporting Information). The protonated, pendant D-cmphH ligands project above and below the planes of these supramolecular layers. Through their unligated carboxylate groups, they engage in hydrogen bonding with aqua ligands in neighboring layers, thus constructing the pseudo 3-D crystal structure of **1** (Figure S2, Supporting Information). Unligated water molecules are held to the 1-D coordination polymer chains by accepting hydrogen bonds from some dpa N−H groups. Geometric parameters for the hydrogen bonding interactions in **1** are listed in Table S2.

Structural Description of {[Cd(D-cmph)(dpa)(Hdpa)]-ClO_4}$_n$ (1a). The asymmetric unit of compound **1a** contains two cadmium atoms on crystallographic 2-fold rotation axes, one complete D-cmph ligand, one dpa ligand, one Hdpa ligand protonated at one of its pyridyl rings, and an unligated perchlorate ion. A very distorted $\{CdO_4N_2\}$ octahedral coordination environment is present at both unique cadmium atoms, with *cis* dpa ligands at Cd1 and *cis* Hdpa ligands at Cd2. Chelating carboxylate groups from two D-cmph ligands occupy the remaining four coordination sites at each cadmium atom (Figure 3). Bond lengths and angles within the coordination spheres of **1a** are listed in Table S1.

Cadmium atoms are bridged by bis(chelating) D-cmph ligands into cationic $[Cd(D\text{-cmph})(dpa)(Hdpa)]_n^{n+}$ coordination polymer chains (Figure 4a), whose metal−metal contact distances are 9.525 Å. These chains form a supramolecular (4,4) zigzag layer via hydrogen bonding donation from all of the protonated Hdpa pyridyl rings in one chain to the pendant

dx.doi.org/10.1021/cg301091f | *Cryst. Growth Des.* 2012, 12, 5125−5137

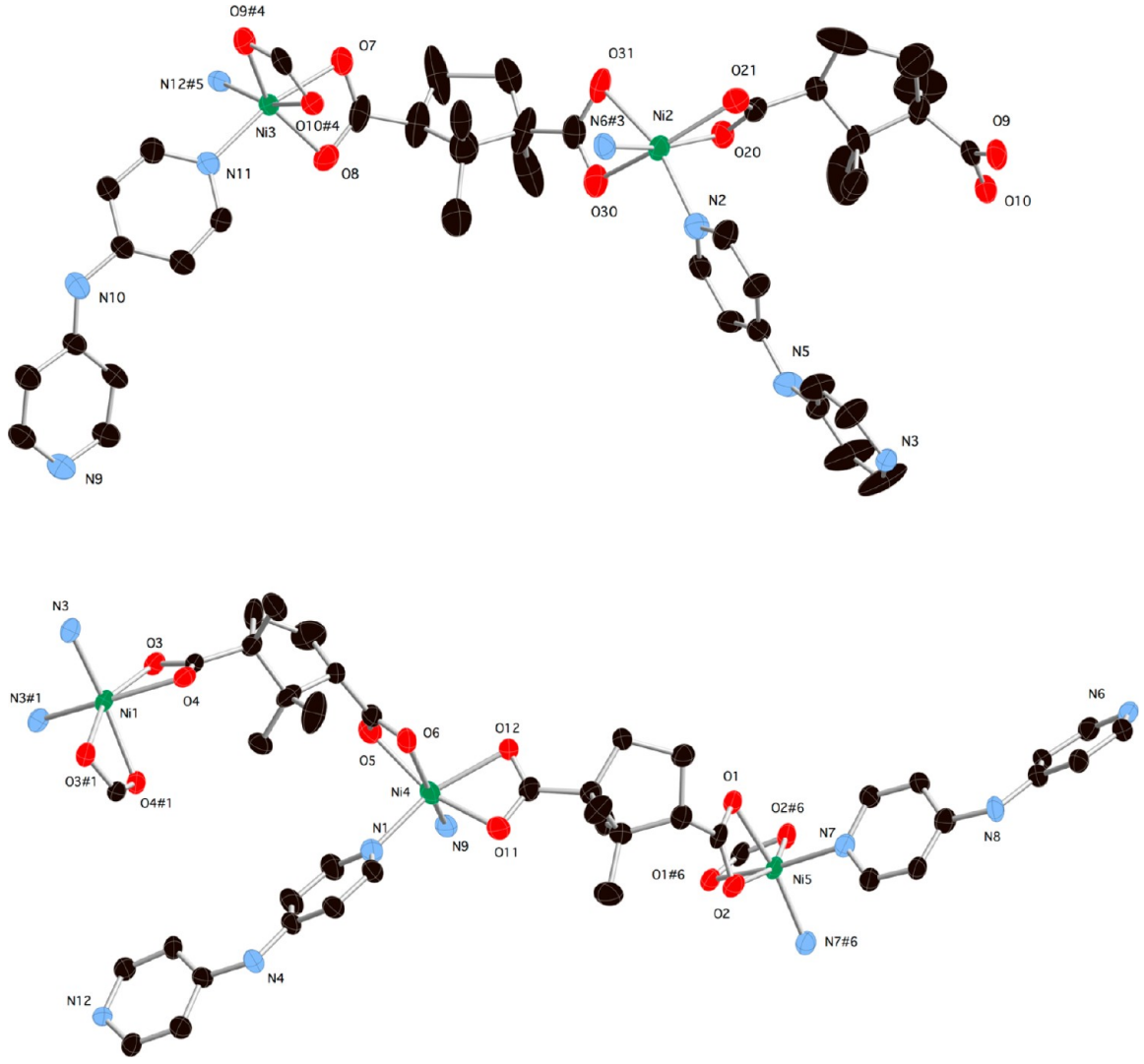

Figure 7. Coordination environments of **3**.

pyridyl groups of the unprotonated dpa ligands in two other chains. The intermetallic separation across the dpa–Hdpa hydrogen bonded pairs is 22.370 Å. Unligated perchlorate ions are held between neighboring layers, by accepting hydrogen bonds from dpa and Hdpa central amine groups, thereby preventing interpenetration of these layer motifs (Figure 4b). Geometric parameters for the hydrogen bonding interactions in **1a** are listed in Table S2.

Structural Description of $[Zn_2(D\text{-cmph})_2(dpa)(H_2O)]_n$ (2). The asymmetric unit of compound **2** contains four divalent zinc atoms, four D-cmph ligands, two dpa ligands, and two bound water molecules. Zinc atoms Zn1 and Zn3 are coordinated in distorted $\{ZnO_4N\}$ square pyramidal environments (τ = 0.22 and 0.25,[20] respectively). In both cases, a chelating D-cmph carboxylate group span axial and equatorial positions. The remaining three coordination sites are taken up by a dpa pyridyl nitrogen donor and *cis* oxygen donors from two other D-cmph ligands. A tetrahedral $\{ZnO_3N\}$ arrangement is seen at both Zn2 and Zn4, with a dpa pyridyl nitrogen donor, an aqua ligand, and oxygen donors from two D-cmph ligands comprising the coordination sphere. Bond lengths and angles within the four distinct coordination environments (Figure 5) are given in Table S3.

Square pyramidally coordinated Zn1 and tetrahedrally coordinated Zn4 atoms are connected into $[Zn_2(D\text{-cmph})_2(H_2O)]_n$ ribbons by chelating/monodentate μ_2-κ^3-*O,O′:O″* bridging and exotridentate μ_3-κ^3-*O:O′:O″* D-cmph ligands (Scheme 2). The Zn1 atoms are bridged in an exobidentate fashion with a metal–metal distance of 9.256 Å, with the related distance between Zn4 atoms being identical. The carboxylate groups of the exotridentate D-cmph ligands link Zn1 and Zn4 atoms in an *anti-syn* manner, providing a metal–metal contact distance of 4.484 Å. Pillaring dpa ligands link Zn1 and Zn4 atoms in neighboring ribbons to construct 2-D $[Zn_2(D\text{-cmph})_2(H_2O)(dpa)]_n$ slabs (Figure 6a). The pyridyl rings of the dpa ligands are twisted by 27.5° relative to each other, yielding a through-ligand metal–metal contact distance of 11.630 Å. The square pyramidally coordinated Zn3 and tetrahedrally coordinated Zn2 atoms are connected into virtually identical $[Zn_2(D\text{-cmph})_2(H_2O)(dpa)]_n$ slabs, with crystallographic distinction fostered only by subtle conformational differences. Here, the *anti-syn* carboxylate bridged Zn···Zn contact distance is 4.466 Å, the through-dpa metal–metal contact distance is 11.521 Å, and the dpa pyridyl ring twist angle is 18.4°.

The underlying topology of the 2-D $[Zn_2(D\text{-cmph})_2(H_2O)(dpa)]_n$ slabs can be derived by treating the square pyramidally

dx.doi.org/10.1021/cg301091f | *Cryst. Growth Des.* 2012, 12, 5125–5137

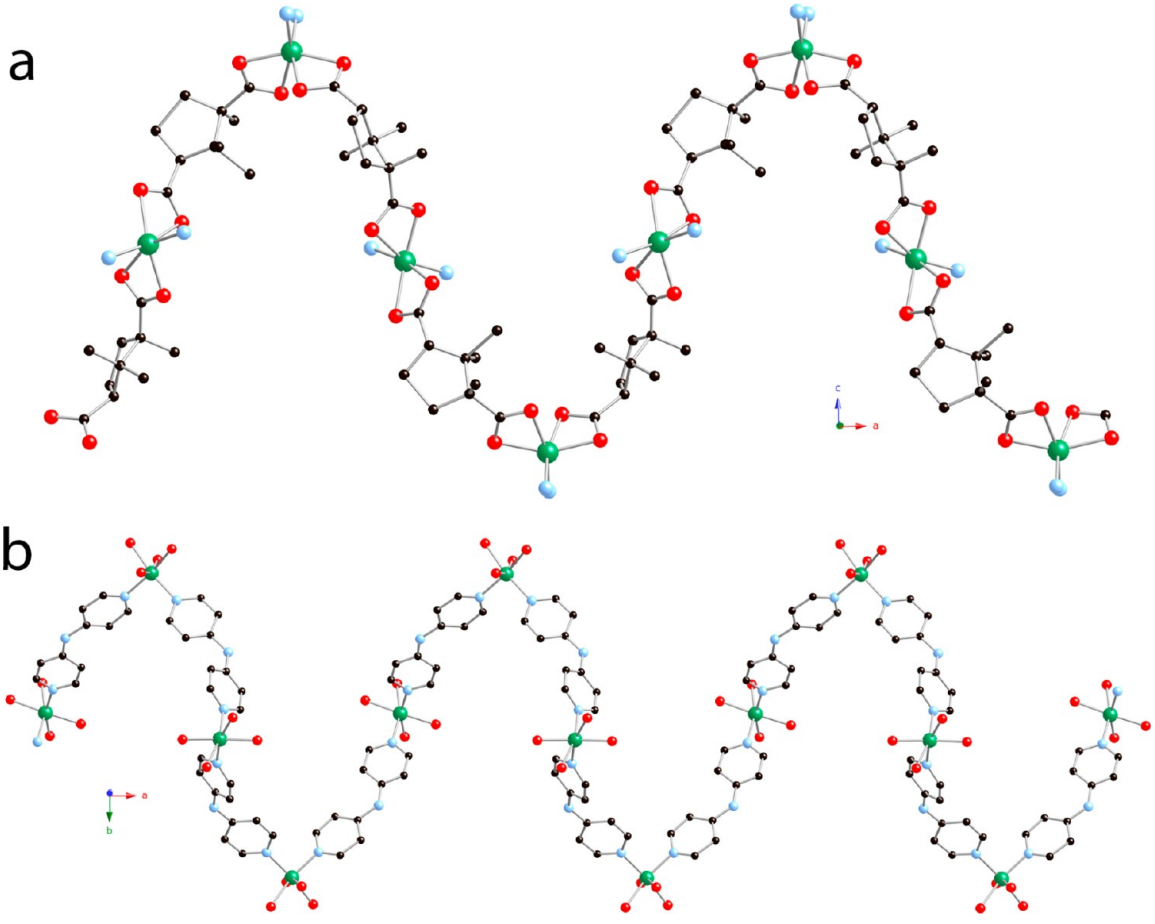

Figure 8. (a) $[Ni(D\text{-cmph})]_n$ chain in **3**. (b) Helical $[Ni(dpa)]_n$ chain in **3**.

coordinated zinc atoms as 4-connected nodes, and the tetrahedrally coordinated zinc atoms and exotridentate D-cmph ligands as 3-connected nodes. According to TOPOS, the resulting 3,4-connected binodal net has a Schläfli symbol of $(5^3)_2(5^48^2)$. A schematic representation of this net, which features five-membered circuits, is shown in Figure 6b. Crystallographically distinct $[Zn_2(D\text{-cmph})_2(H_2O)(dpa)]_n$ slabs interact through hydrogen bonding donation from dpa central amine groups to unligated D-cmph carboxylate oxygen atoms. In contrast, crystallographically identical $[Zn_2(D\text{-cmph})_2(H_2O)(dpa)]_n$ slabs engage in hydrogen bonding mechanisms involving the aqua ligands and unligated D-cmph carboxylate oxygen atoms. Metrical parameters for these supramolecular interactions are given in Table S2. The slabs stack in a *BAA′B′* pattern along the *c* crystal direction (Figure S3, Supporting Information).

Structural Description of $\{[Ni(D\text{-cmph})(dpa)]\cdot 3H_2O\}_n$ (3). The rather large asymmetric unit of compound **3** contains five crystallographically distinct divalent nickel atoms, two of which (Ni1, Ni5) are situated on crystallographic 2-fold axes, along with 4 unique D-cmph ligands, 4 dpa ligands, and 12 disordered water molecules of crystallization (according to a calculation with SQUEEZE, and consistent with thermogravimetric analysis). All of the nickel atoms have distorted $\{NiO_4N_2\}$ octahedral coordination spheres (Figure 7), with chelating carboxylate groups from two D-cmph ligands located across axial and equatorial sites. The remaining *cis* coordination positions are taken up by dpa pyridyl nitrogen donor atoms. Slight differences in coordination sphere bond lengths and angles (Table S4) and organic ligand conformation result in the crystallographic distinction among the nickel atoms.

Nickel atoms Ni2 and Ni3 are linked together by bis(chelating) D-cmph ligands to form $[Ni(D\text{-cmph})]_n$ chains (Figure 8a), whose Ni···Ni contact distances are 8.947 and 9.026 Å. Very similar $[Ni(D\text{-cmph})]_n$ chains are formed by the linkage of Ni1, Ni4, and Ni5 atoms by crystallographically distinct bis(chelating) D-cmph ligands. The Ni···Ni internuclear distances in these chains are 8.900 and 9.024 Å. Differences between the metal−metal contact distances are caused by variances in the conformations of the carboxylate groups within the D-cmph ligands. The nickel atoms in **3** are also connected by dpa tethers, which construct helical $[Ni(dpa)]_n$ chains (Figure 8b). The four crystallographically distinct dpa ligands, with slightly different dihedral angles between their pyridyl ring planes, provide Ni···Ni contact distances of 11.233, 11.261, 11.470, and 11.640 Å.

Each $[Ni(D\text{-cmph})]_n$ chain is connected to four other parallel $[Ni(D\text{-cmph})]_n$ chains by the dpa tethers, resulting in a 3-D $\{[Ni(D\text{-cmph})(dpa)]_n$ coordination polymer network (Figure 9a). Rectangular channels within this net, bracketed by dpa ligands and defined by through-space Ni···Ni distances of 15.6 and 18.2 Å, accommodate a second $\{[Ni(D\text{-cmph})(dpa)]_n$ network. According to TOPOS, this 4-connected net has a 2-fold interpenetrated 4^28^4 **lvt** topology (Figure 9b). Some previous examples of this relatively uncommon 4-connected network include $[Pb_3Cl_3(OH)(succinate)]_n$,[21a] $\{[Cu(4,4'\text{-bpy})_2(O_3SCF_3)_2]\cdot 2CH_2Cl_2\cdot 2H_2O\}_n$,[21b] and $\{[Cu(oxybisbenzoate)(H_2O)]_2\cdot 0.5H_2O\}_n$,[21c]

dx.doi.org/10.1021/cg301091f | *Cryst. Growth Des.* 2012, 12, 5125−5137

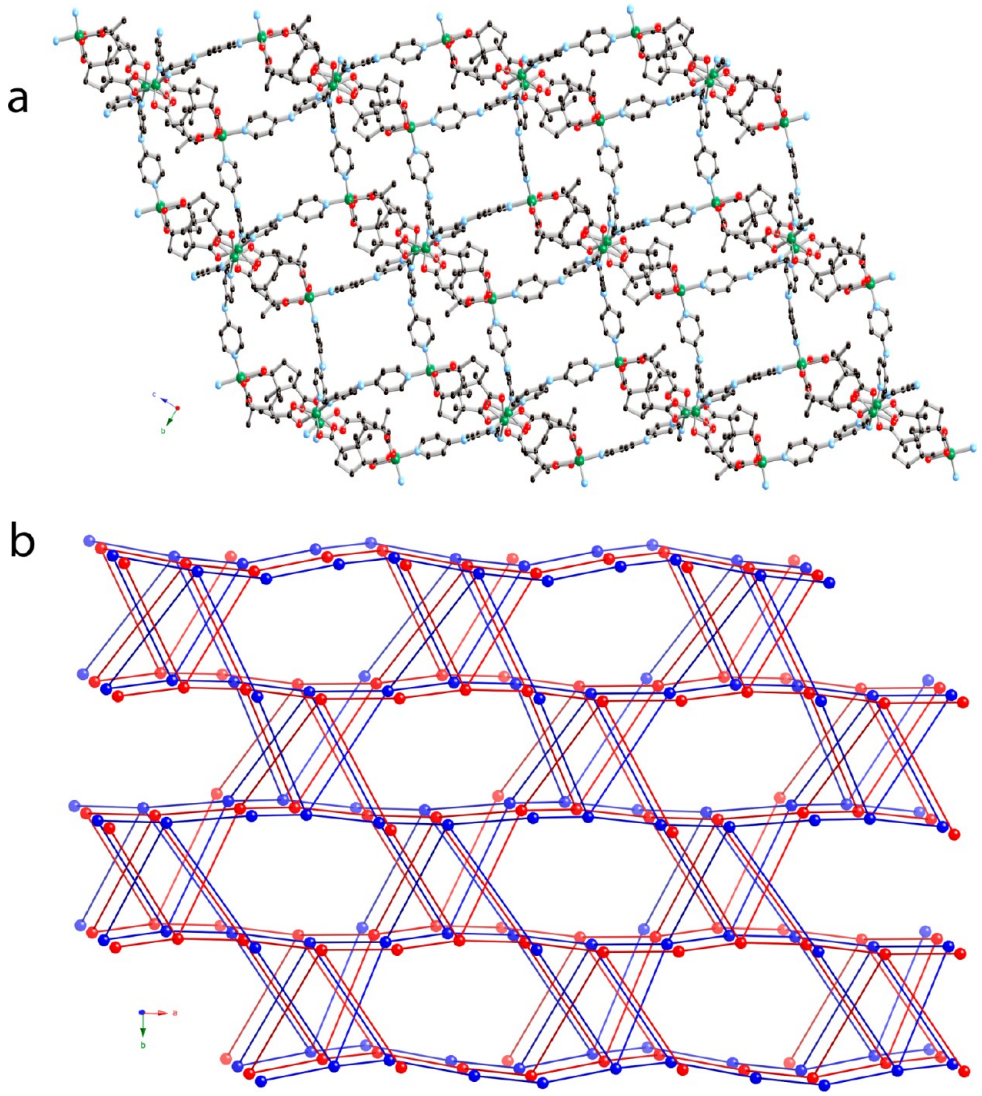

Figure 9. (a) A single 3-D $\{[Ni(D\text{-cmph})(dpa)]_n$ coordination polymer network in **3**. (b) 2-fold interpenetration of 4-connected 4^28^4 **lvt** topology networks in **3**.

which show non-interpenetration, 2-fold interpenetration, and 5-fold interpenetration, respectively. Compound **3** appears to be only the second known example of a 2-fold interpenetrated **lvt** topology, to the best of our knowledge. Disordered water molecules of crystallization occupy the extra-framework incipient void space in **3**, totaling 16.9% of the unit cell volume according to a calculation with PLATON.[17]

Structural Description of $\{[Co_2(D\text{-cmph})_2(dpa)]\cdot H_2O\}_n$ (4) and $\{[Cu_2(D\text{-cmph})_2(dpa)]\cdot H_2O\}_n$ (5). As compounds **4** and **5** are essentially isostructural, only the structural details for **4** will be discussed in detail. Its asymmetric unit consists of two divalent cobalt atoms, two D-cmph ligands, and two halves of dpa ligands whose central amine groups are located on crystallographic 2-fold rotation axes. In both **4** and **5** the coordination environments at the metal atoms are $\{MO_4N\}$ square pyramids with different degrees of deviation from ideal geometry (τ = 0.058 and 0.008 at Co1 and Co2 in **4**, τ = 0.127 and 0.122 at Cu1 and Cu2 in **5**). In all cases the oxygen donors from four different D-cmph fill the equatorial positions, with a dpa pyridyl nitrogen donor resting in the axial position (Figure 10). Four D-cmph carboxylate groups bridge equatorial positions of both Co1 and Co2 to construct $\{Co_2(OCO)_4\}$ paddlewheel dinuclear units, in which the Co···Co through-space distance is 2.8606(12) Å. The related Cu···Cu distance in **5** is 2.6743(18) Å. Bond lengths and angles within the coordination spheres of **4** and **5** are listed in Table S5.

The exotetradentate D-cmph ligands with a μ_4-κ^4O:O':O'':O''' binding mode connect $\{Co_2(OCO)_4\}$ paddlewheel units into $[Co_2(D\text{-cmph})_2]_n$ (4,4) grid coordination polymer layers (Figure 11a), with each dinuclear unit acting as a 4-connected node. Parallel $[Co_2(D\text{-cmph})_2]_n$ (4,4) grid layers are pillared into a 3-D $\{[Co_2(D\text{-cmph})_2(dpa)]_n$ network by dipodal dpa ligands, which span a Co···Co distance of 11.295 Å in **4**, with the related metal−metal contact distance in **5** being slightly shorter, at 11.219 Å. The resulting 6-connected networks of **4** and **5** have a simple non-interpenetrated $4^{12}6^3$ **pcu** primitive cubic topology (Figure 11b), in contrast to the self-penetrated 4^86^68 6-connected **rob** network seen in an analogous phase $[Co_2(D\text{-cmph})_2(4,4'\text{-bipyridine})]_n$ where virtually identical $[Co_2(D\text{-cmph})_2]_n$ layers are cross-pillared by rigid rod 4,4′-bipyridine ligands.[9e] A related phase containing the even longer rod-like dipyridyl ligand bis(4-pyridylmethyl)piperazine (bpmp), $[Co_2(D\text{-cmph})_2(bpmp)]_n$, exhibits a different self-penetrated $4^46^{10}8$ **mab** 6-connected topology.[22] It is

dx.doi.org/10.1021/cg301091f | *Cryst. Growth Des.* 2012, 12, 5125−5137

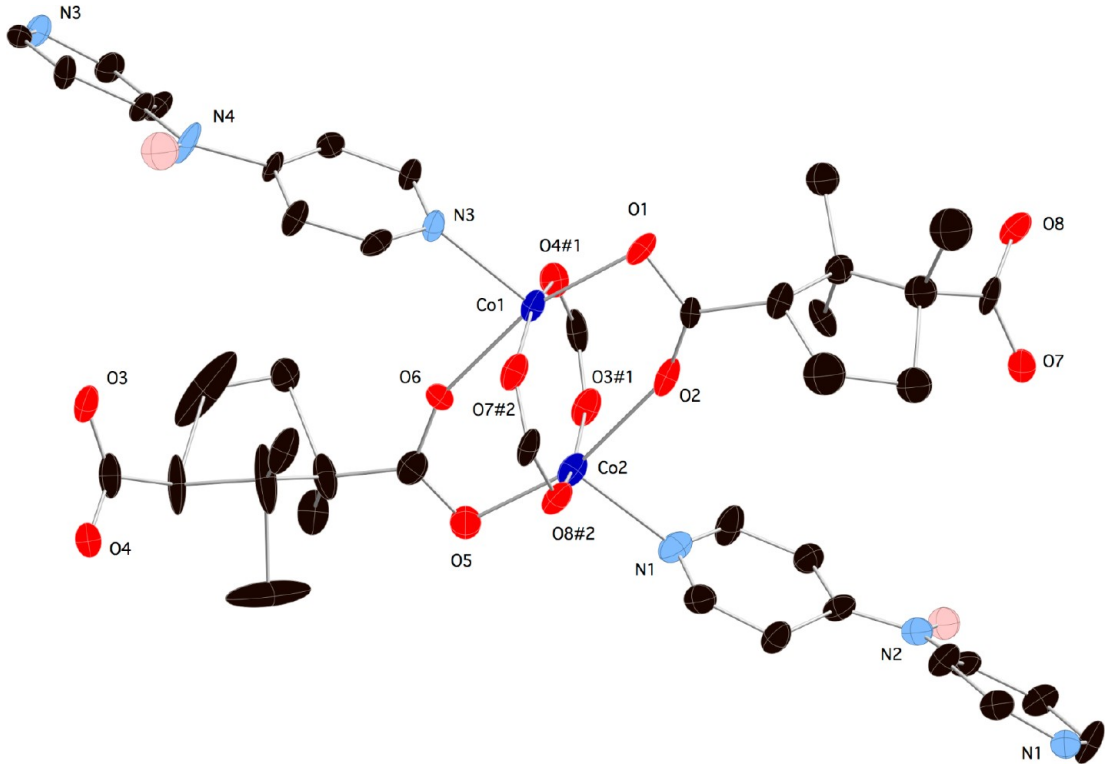

Figure 10. Coordination environments of **4**, showing a complete $\{Co_2(OCO)_4\}$ paddlewheel dinuclear unit. Similar clusters are evident in the copper derivative **5**.

possible that the relatively short length and the kinked disposition of the pyridyl nitrogen donor atoms in the dpa ligands in **4** permit the self-assembly of the non-self-penetrated **pcu** net in lieu of any 6-connected self-penetrated topology. Isolated water molecules of crystallization, hydrogen-bonded to the dpa central amine groups, occupy the extra-framework space comprising 6.0% of the unit cell volume of **4** (5.4% for **5**).

Magnetic Properties of 4 and 5. Variable temperature magnetic susceptibility studies were carried out to investigate spin communication within the equatorial-equatorial bridged paddlewheel dimers in **4** and **5**. For **4**, the $\chi_m T$ product of 2.37 cm^3 mol^{-1} Co at 300 K is higher than that expected for a spin-only $S = 3/2$ ion because of orbital contributions to the magnetic moment. A slow decrease in $\chi_m T$ product value occurs between 300 and 100 K, at which point the value is 2.16 cm^3-K mol^{-1} Co. Below 100 K the $\chi_m T$ product decreases more rapidly, reaching 0.12 cm^3-K mol^{-1} Co at 2 K. The shape of the $\chi_m T(T)$ graph (Figure 12) is indicative of antiferromagnetic coupling between paramagnetic cobalt ions in **4**, although zero-field splitting is also known to reduce the $\chi_m T$ product as temperature decreases due to population of Kramers doublets.[13] The data were fit to Rueff's expression[23] for a chain of $S = 3/2$ ions (eq 1), which is also effective for divalent cobalt dimers and takes magnetic superexchange (J) and single-ion effects such as zero-field splitting (D) into account, affording values of $A = 1.51(4)$, $B = 1.07(5)$, $g = 2.39(5)$, $D = 20.1(7)$ cm^{-1}, and $J = -3.6(2)$ cm^{-1} with $R = \{\Sigma[(\chi_m T)_{obs} - (\chi_m T)_{calc}]^2\}^{1/2} = 6.0 \times 10^{-4}$. The values for g and J in **4** correspond rather closely to those in $[Co_2(D\text{-cmph})_2(bpmp)]_n$ ($g = 2.328(8)$, $J = -3.9(1)$ cm^{-1}), which possesses similar $[Co_2(D\text{-cmph})_2]_n$ layers with embedded $\{Co_2(OCO)_4\}$ paddlewheel dimers. In both **4** and $[Co_2(D\text{-cmph})_2(bpmp)]_n$, the dipyridyl ligand is too long to mediate any tangible spin communication, resulting in similar magnetic behavior.

$$\chi_m T = A \exp(-D/kT) + B \exp(J/kT) \quad (1)$$

where $A + B = C = (5Ng^2\beta^2/4k)$.

For **5**, the $\chi_m T$ product of 0.26 cm^3-K mol^{-1} Cu at 300 K is lower than that expected for an uncoupled $S = 1/2$ ion. The $\chi_m T$ product decreased rapidly upon cooling, reaching 0.078 cm^3-K mol^{-1} Cu at 100 K and 0.00064 cm^3-K mol^{-1} Cu at 26 K. Both of these features indicate strong antiferromagnetic coupling, a common feature of equatorial-equatorial bridged $\{Cu_2(OCO)_4\}$ paddlewheel dimers.[13] The data were fit (Figure 13) to the Bleaney–Bowers expression for an interacting pair of $S = 1/2$ ions (eq 2),[24] giving $g = 1.91(2)$ and $J = -202(5)$ cm^{-1} with $R = 4.0 \times 10^{-5}$. Direct through-space exchange between the magnetic $d_{x^2-y^2}$ orbitals within the dimeric kernels is responsible for the very strong antiferromagnetic coupling in **5**. The differing orbital populations in **4** result in a reduction of the magnitude of the overall antiferromagnetic coupling.

$$\chi_m T = \left(\frac{Ng^2\beta^2}{3k}\right)\left[1 + \left\{\frac{1}{3}\exp(J/kT)\right\}\right]^{-1} \quad (2)$$

Luminescence Spectra of 1/1a and 2. Irradiation of crystalline samples of the d^{10} metal coordination polymers **1**/**1a** (as an inseparable mixture) and **2** with ultraviolet light (λ_{ex} = 225 nm) in the solid state resulted in modest blue-violet visible light emission whose spectral maxima were observed within the ultraviolet region (λ_{max} = 395 nm for **1**/**1a**; λ_{max} = 375 nm for **2**, Figures S4–S5, Supporting Information). As seen in other divalent cadmium or zinc coordination polymers with aromatic ligands,[25] this fluorescent behavior can likely be ascribed to ligand-centered $\pi-\pi^*$ or $\pi-n$ electronic

dx.doi.org/10.1021/cg301091f | *Cryst. Growth Des.* 2012, 12, 5125–5137

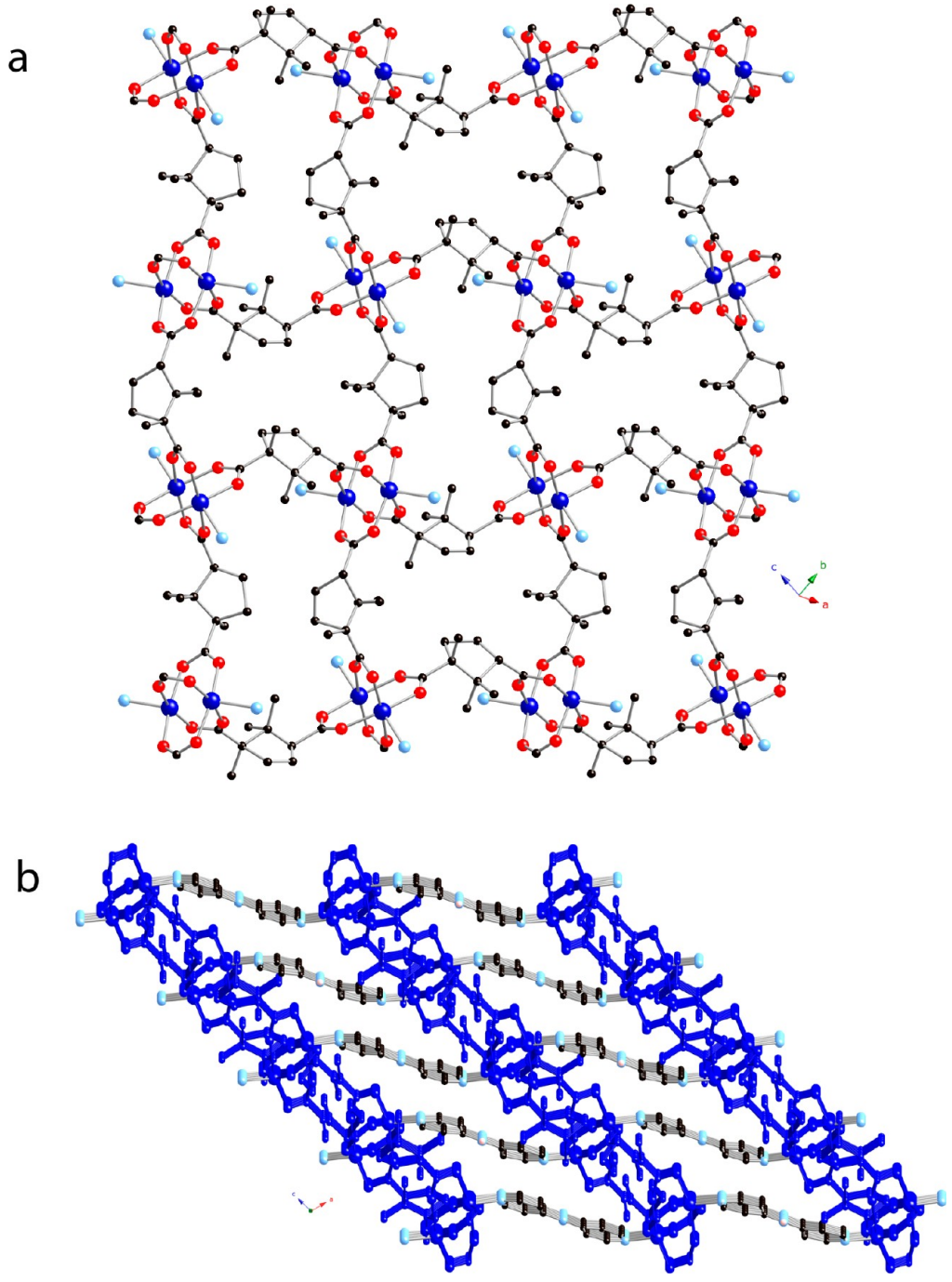

Figure 11. (a) $[Co_2(D\text{-cmph})_2]_n$ (4,4) grid coordination polymer layer in **4**. (b) 3-D $\{[Co_2(D\text{-cmph})_2(dpa)]_n$ network in **4**, with $[Co_2(D\text{-cmph})_2]_n$ layers shown in blue.

transitions within the molecular orbital manifolds of any aromatic ligands. Here, the pyridyl groups of the dpa ligands serve this role. A crystalline sample of the pure dpa ligand itself emits violet light (λ_{max} = 395 nm) upon excitation with 240 nm ultraviolet light (Figure S6), thereby corroborating the origin of the emissive properties of **1**/**1a**, and **2**.

Thermal Properties. Samples of compounds **2**−**5** were subjected to thermogravimetric analysis to examine their dehydration and thermal degradation behaviors (Figures S6−S9, Supporting Information). Due to the explosive nature of perchlorate compounds, the mixture **1** of **1a** was not subjected to thermogravimetric analysis. The aqua ligands of compound **2** were ejected between 180 and 230 °C, with the observed mass loss of 2.9% corresponding well to the predicted loss (2.5%). The mass was largely stable until 230 °C, whereupon the organic ligands were combusted. Compound **3** underwent dehydration between 30 and 105 °C, with the mass loss of 11.3% consistent with elimination of three water molecules per nickel atom (11.2% calc'd). Destruction of the coordination polymer network occurred at 360 °C, marked by a large and rapid mass loss. Compound **4** exhibited loss of its water molecules of crystallization between 120 and 160 °C, indicated by a 2.4% mass loss (2.6% calc'd). The mass remained steady until 415 °C, at which point ejection of the organic ligands occurred. Compound **5** dehydrated between 70 and 110 °C, by which point 2.2% of the original mass was lost (2.5% calc'd).

dx.doi.org/10.1021/cg301091f | *Cryst. Growth Des.* 2012, 12, 5125−5137

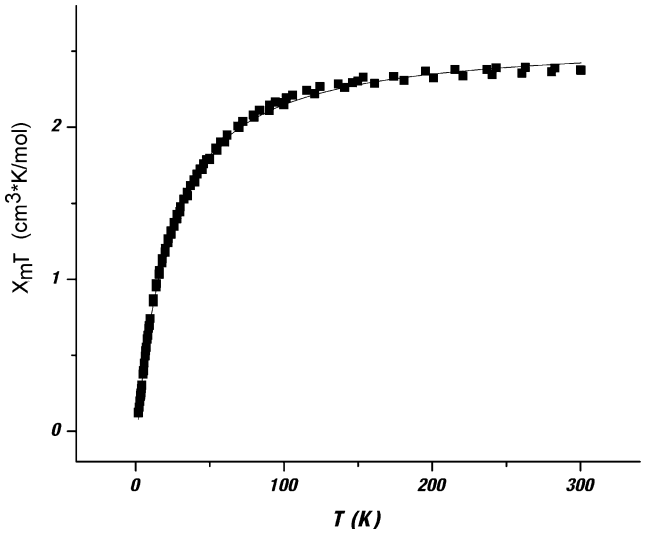

Figure 12. $\chi_m T$ vs T plot for **4**. The dark line represents the best fit to eq 1.

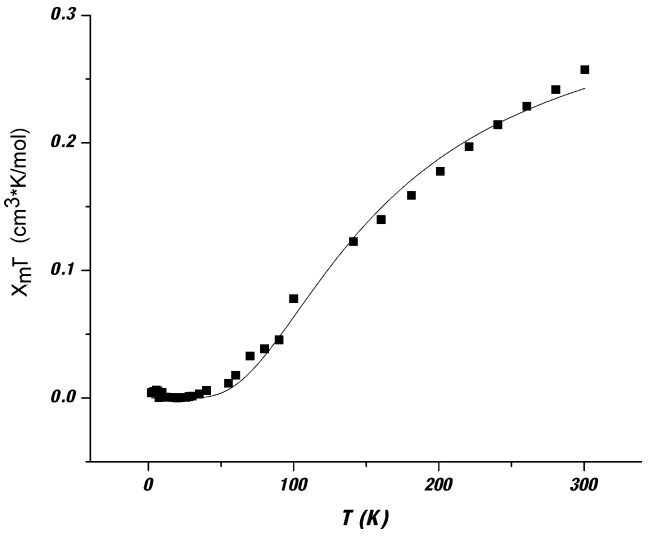

Figure 13. $\chi_m T$ vs T plot for **5**. The dark line represents the best fit to eq 2.

The mass then held nearly constant until combustion of the organic components at 275 °C. From an examination of the temperatures at which the organic ligands were ejected, it is likely that the 3-D coordination polymers **3**, **4**, and **5** have a higher thermal stability than that of the 2-D coordination polymer **2**.

CONCLUSIONS

Coordination geometry preferences play an extremely large role in structure direction in a series of chiral divalent metal D-camphorate coordination polymers with 4,4′-dipyridylamine coligands. Major differences between the cadmium derivatives **1** and **1a** rest in the different coordination environments (pentagonal bipyramidal in **1**, octahedral in **1a**), and in the different disposition of the dpa ligands (trans in **1**, cis in **1a**). In **1**, the trans dpa ligands propagate the 1-D coordination polymer chain motifs, while this role is served by fully deprotonated D-cmph ligands in **1a**. Mixed tetrahedral and square pyramidal coordination environments in the zinc derivative **2** produce a chiral 2-D layer, albeit one with a new 3,4-connected binodal topology. Octahedral coordination spheres in the nickel derivative **3**, with two chelating D-camphorate carboxylate groups, produce a rarely observed 4-connected interpenetrated **lvt** network. Square pyramidal coordination environments within commonly seen paddlewheel clusters produce metal dicarboxylate layers in **4** and **5**, observed in other cobalt D-camphorate coordination polymers. As in previously reported related derivatives, the paddlewheel clusters in both **4** and **5** mediate antiferromagnetic coupling between the paramagnetic metal ions. Differences in antiferromagnetic coupling (weak in **4**, strong in **5**) can be ascribed to different *d* orbital populations for divalent cobalt versus divalent copper. Pillaring of the metal D-camphorate layer motifs by the kinked dipyridylamine ligands produces a simple $4^{12}6^3$ **pcu** net in both the copper and cobalt derivatives, in lieu of possible self-penetrated 6-connected nets observed in some previously reported dual-ligand cobalt D-camphorate coordination polymers. Coordination polymers in this series with 3-D connectivity (**3**, **4**, **5**) have higher thermal stability than the 2-D zinc analogue **2**.

ASSOCIATED CONTENT

Supporting Information

Hydrogen bonding information, stacking diagrams for **1** and **2**, luminescence spectra, crystallographic data files, and thermogravimetric analysis graphs. This material is available free of charge via the Internet at http://pubs.acs.org. Crystallographic data (excluding structure factors) for **1**–**5** have been deposited with the Cambridge Crystallographic Data Centre with Nos. 894374 (**1**), 812461 (**1a**), 812465 (**2**), 812464 (**3**), 812462 (**4**), and 812463 (**5**). Copies of the data can be obtained free of charge via the Internet at http://www.ccdc.cam.ac.uk/conts/retrieving.html or by post at CCDC, 12 Union Road, Cambridge CB2 1EZ, U.K. (Fax: 44-1223336033, Email: deposit@ccdc.cam.ac.uk).

AUTHOR INFORMATION

Corresponding Author

*Mailing address: Lyman Briggs College, E-30 Holmes Hall, 919 East Shaw Lane, Michigan State University, East Lansing, MI 48825 USA. E-mail: laduca@msu.edu.

Notes

The authors declare no competing financial interest.

ACKNOWLEDGMENTS

We acknowledge the donors of the American Chemical Society Petroleum Research Fund for funding this work. We thank Ms. Julie A. Wilson and Mr. Peter Kraft for experimental assistance in spectra acquisition.

REFERENCES

(1) (a) Murray, L. J.; Dinca, M.; Long, J. R. *Chem. Soc. Rev.* **2009**, *38*, 1294–1314. and references therein. (b) Han, S. S.; Mendoza-Cortes, J. L.; Goddard, W. A. *Chem. Soc. Rev.* **2009**, *38*, 1460–1476 and references therein.

(2) Li, J. R.; Kuppler, R. J.; Zhou, H. C. *Chem. Soc. Rev.* **2009**, *38*, 1477–1504 and references therein.

(3) (a) Plabst, M.; McCusker, L. B.; Bein., T. *J. Am. Chem. Soc.* **2009**, *131*, 18112–18118. (b) Liu, Y.; Kravtsov, V. C.; Eddaoudi, M. *Angew. Chem., Int. Ed.* **2008**, *47*, 8446–8449. (c) Nouar, F.; Eckert, J.; Eubank, J. F.; Forster, P.; Eddaoudi, M. *J. Am. Chem. Soc.* **2009**, *131*, 2864–2870.

(4) (a) Lee, J.; Farha, O. K.; Roberts, J.; Scheidt, K. A.; Nguyen, S. T.; Hupp, J. T. *Chem. Soc. Rev.* **2009**, *38*, 1450–1459. and references

therein. (b) Ma, L.; Abney, C.; Lin, W. *Chem. Soc. Rev.* **2009**, *38*, 1248−1256 and references therein.
(5) (a) Zang, S.; Su, Y; Li, Y.; Ni, Z.; Meng, Q. *Inorg. Chem.* **2006**, *45*, 174−180. (b) Wang, L.; Yang, M.; Li, G.; Shi, Z.; Feng, S. *Inorg. Chem.* **2006**, *45*, 2474−2478.
(6) (a) Cheetham, A. K.; Rao, C. N. R.; Feller, R. K. *Chem. Commun.* **2006**, 4780−4795. and references contained therein. (b) Blatov, V. A.; Carlucci, L.; Ciani, G.; Proserpio, D. M. *CrystEngComm* **2004**, *6*, 377−395 and references contained therein.
(7) Kurmoo, M. *Chem. Soc. Rev.* **2009**, *38*, 1353−1379 and references therein.
(8) (a) Wu, C; Lin., W. *Angew. Chem., Int. Ed.* **2007**, *46*, 1075−1078. (b) Vaidhyanathan, R.; Bradshaw, D.; Rebilly, J.; Barrio, J.; Gould, J. A.; Berry, N.; Rosseinsky, M. J. *Angew. Chem., Int. Ed.* **2006**, *45*, 6495−6499.
(9) (a) Zhang, J.; Chew, E.; Chen, S.; Pham, J. T. H.; Bu, X. *Inorg. Chem.* **2008**, *47*, 3495−3497. (b) Zhang, J.; Bu, X. *Angew. Chem., Int. Ed.* **2007**, *46*, 6115−6118. (c) Li, F.; Kang, Y.; Dai, Y.; Zhang, J. *Inorg. Chem. Commun.* **2011**, *14*, 228−230. (d) Wu, J.; Huang, S. *CrystEngComm* **2011**, *13*, 2062−2070. (e) Zhang, J.; Yao, Y.; Bu, X. *Chem. Mater.* **2007**, *19*, 5083−5089. (f) Chen, Z.; Lin, Z.; Stips, T.; Dehnen, S. *Inorg. Chem. Commun.* **2011**, *14*, 137−139.
(10) (a) Zhang, J.; Bu, X. *Chem. Commun.* **2008**, 444−446. (b) Zhang, J.; Bu, X. *Chem. Commun.* **2009**, 206−208.
(11) (a) Shyu, E.; Supkowski, R. M.; LaDuca, R. L. *Inorg. Chem.* **2009**, *48*, 2723−2725. (b) Braverman, M. A.; Nettleman, J. H.; Supkowski, R. M.; LaDuca, R. L. *Inorg. Chem.* **2009**, *48*, 4918−4926. (c) Sasa, M.; Tanaka, K.; Bu, X.-H.; Shiro, M.; Shionoya, M. *J. Am. Chem. Soc.* **2001**, *123*, 10750. (d) Chun, H. P.; Bernal, I. *Cryst. Growth Des.* **2001**, *1*, 67. (e) Kauffman, G. B.; Bernal, I.; Schutt, H. W. *Enantiomer* **1999**, *4*, 33.
(12) Zapf, P. J.; LaDuca, R. L.; Rarig, R. S.; Johnson; Zubieta, K. M. J. *Inorg. Chem.* **1998**, *37*, 3411−3414.
(13) Kahn, O. *Molecular Magnetism*; VCH Publishers: New York, 1993.
(14) *SAINT, Software for Data Extraction and Reduction*, Version 6.02; Bruker AXS, Inc.: Madison, WI, 2002.
(15) *SADABS, Software for Empirical Absorption Correction*, Version 2.03; Bruker AXS, Inc.: Madison, WI, 2002.
(16) Sheldrick, G. M. *SHELXTL, Program for Crystal Structure Refinement*; University of Göttingen: Gottingen, Germany, 1997.
(17) Spek, A. L. *PLATON, A Multipurpose Crystallographic Tool*; Utrecht University: Utrecht, The Netherlands, 1998.
(18) (a) Bernardinelli, G.; Flack, H. D. *Acta Crystallogr.* **1985**, *A41*, 500. (b) Flack, H. D. *Acta Crystallogr.* **1983**, *A29*, 876.
(19) Blatov, V. A.; Shevchenko, A. P.; Serezhkin, V. N. *J. Appl. Crystallogr.* **2000**, *33*, 1193. TOPOS software is available for download at http://www.topos.ssu.samara.ru.
(20) Addison, A. W.; Rao, T. N. J.; Reedijk, J.; van Rijn, J.; Verschoor, G. C. *J. Chem. Soc., Dalton Trans.* **1984**, 1349−1356.
(21) (a) Zhang, H.; Kang, Y.; Tan, Y.; Wang, F. *Inorg. Chem. Commun.* **2011**, *14*, 197−199. (b) Carlucci, L.; Cozzi, N.; Ciani, G.; Moret, M.; Proserpio, D.; Rizzato, S. *Chem. Commun.* **2002**, 1354−1355. (c) Wang, X. L.; Chao, Q.; Wang., E.; Li, Y.; Su, Z. *Chem. Commun.* **2005**, 5450−5452.
(22) Blake, K. M.; LaDuca, R. L. *Inorg. Chem. Commun.* **2011**, *14*, 1250−1253.
(23) Rueff, J. M.; Masciocchi, N.; Rabu, P.; Sironi, A.; Skoulios, A. *Eur. J. Inorg. Chem.* **2001**, 2843−2848.
(24) Bleaney, B.; Bowers, K. D. *Proc. R. Soc. London, Ser. A.* **1952**, *214*, 451.
(25) Allendorf, M. D.; Bauer, C. A.; Bhakta, R. K.; Houk, R. T. J. *Chem. Soc. Rev.* **2009**, *38*, 1330−1352 and references therein.